Relaxation times in a bistable system with parametric, white noise: Theory and experiment

J. M. Sancho
Departamento de Física Teórica, Universidad de Barcelona, 08028 Barcelona, Spain

R. Mannella and P. V. E. McClintock
Department of Physics, University of Lancaster, Lancaster LA1 4YB, United Kingdom

Frank Moss
Department of Physics, University of Missouri—St. Louis, St. Louis, Missouri 63121

(Received 22 July 1985)

We consider the effects of external, multiplicative white noise on the relaxation time of a general representation of a bistable system from the points of view provided by two, quite different, theoretical approaches: the classical Stratonovich decoupling of correlations and the new method due to Jung and Risken. Experimental results, obtained from a bistable electronic circuit, are compared to the theoretical predictions. We show that the phenomenon of critical slowing down appears as a function of the noise parameters, thereby providing a correct characterization of a noise-induced transition.

I. INTRODUCTION

A. General

Nonlinear systems with control parameter driven instabilities, and in particular bistable systems with multiplicative (or state-dependent) noise, have motivated a great deal of study in recent years.[1–9] These studies have been particularly important to the understanding of optical bistability[10–14] and to bistability in other systems.[2,3,15,16] An important characteristic of macroscopic, multistable systems is the relaxation time,[17] which indicates critical slowing down near an instability.

In this paper we discuss the relaxation time of a general bistable process represented by a stochastic differential equation

$$\dot{X}=f(X)+g(X)\sigma\xi(t)=F(X,t)\ , \tag{1.1}$$

where

$$f(X)=-X^3+\lambda X^2-QX+R \tag{1.2a}$$

and

$$g(X)=X^2\ . \tag{1.2b}$$

The parametric noise has been introduced into the control parameter λ as $\lambda_t=\lambda+\sigma\xi_t$, where $\sigma\xi_t$ is a Gaussian, white noise of zero mean and variance σ^2, defined by the correlation

$$\langle\xi(t)\xi(t')\rangle=\sigma^2\delta(t-t')\ , \tag{1.3}$$

and where Q and R are constants. This system exhibits bistability only as a function of the mean value λ, of the control parameter and the noise intensity σ.

Since the correlation function $C(s)$ of the response of such a system is not expected to be an exponential with a well-defined correlation time, we define the relaxation time

$$T=\int_0^\infty ds\, C_2(s)/C_2(0) \tag{1.4}$$

following Hernandez-Machado *et al.*[17] The correlation is

$$C_2(s)=\langle\delta X(t+s)\delta X(t)\rangle\ , \tag{1.5}$$

where the deviation is $\delta X(t)=X(t)-\langle X(t)\rangle$, and stationary properties are achieved in the usual way as limits for $t\to\infty$.

Three theoretical methods are used to evaluate T as a function of σ and λ for a specific numerical example of Eq. (1.2). These methods, which are reviewed in Sec. II, are (1) a deterministic approximation, (2) the well-known and often-used decoupling of correlations due to Stratonovich,[18] and (3) a quite recent, exact result obtained by Jung and Risken.[19] Finally, in Sec. III we describe experimental measurements of T obtained from an electronic circuit which models Eq. (1.2), and the data are compared to the theoretical predictions.

B. The model

In order to obtain quantitative results, we have chosen $Q=3$ and $R=0.7$ in Eq. (1.2). These choices result in a bistable region located in the control parameter range $3.2<\lambda<3.7$ for $\sigma=0$. In this range there are one unstable and two stable steady states. Outside this range only one steady state is dynamically accessible for $\lambda>0$. The deterministic response is shown in Fig. 1 by the solid curve with closed circles. (The circles are the measured response for $\sigma=0$ of the electronic circuit described below.) When $\sigma>0$, the variable X is a continuous stochastic process whose probability density $P(X,t)$ obeys the Fokker-Planck equation

$$\partial P(X,t)/\partial t=L(X,t)P(X,t)\ , \tag{1.6}$$

with evolution operator

 ©1985 The American Physical Society

$$L(X,t)=-\frac{\partial}{\partial X}(-X^3+\lambda X^2-QX+R+\sigma^2X^3)+\frac{\sigma^2}{2}\frac{\partial^2X^4}{\partial X^2}\,, \tag{1.7}$$

corresponding to the Stratonovich interpretation of Eq. (1.1).[18,20] The time-independent ($\partial/\partial t=0$) solution of Eqs. (1.6) and (1.7) results in the stationary probability density

$$P_{\rm st}=NX^{-2(1+1/\sigma^2)}\times\exp[(2/\sigma^2)(-\lambda/X+Q/2X^2-R/3X^3)]\,, \tag{1.8}$$

where N is a normalizing constant. It is worth noting that $P_{\rm st}$ has been previously measured experimentally for the present numerical model ($Q=3$, $R=0.7$) on the same electrical circuit described below.[21] For $X\to 0$, $P_{\rm st}$ is a strongly decaying function, but for $X\to\infty$, $P_{\rm st}\sim X^{-2(1+1/\sigma^2)}$, which means that for a finite value of σ, higher-order moments do not exist because they diverge. Specifically, if we define

$$n_0=2/\sigma^2+1\,, \tag{1.9}$$

then all the moments $\langle X^n\rangle$ for $n>n_0$ diverge, so that for $\sigma^2>2$ only $\langle X\rangle$ is finite. For this reason, we expect the Stratonovich approximation to be even less accurate in the present application than in models for which the noise multiplies only the linear term in Eq. (1.2) resulting in finite higher-order moments.

An important property of $P_{\rm st}(X)$ is that its extrema are shifted in relation to λ when $\sigma>0$.[21,22] The locations of the extrema X_m are given by the roots of

$$(1+\sigma^2)X_m^3-\lambda X_m^2+QX_m-R=0\,. \tag{1.10}$$

For $\lambda>0$, this cubic has three real roots (corresponding to a bimodal density) for $\sigma<\sigma_c\cong 1.02$, but only one real root for $\sigma>\sigma_c$ (monomodal density). Bistability can therefore be induced or destroyed by varying the noise intensity for fixed λ. This is one example of the noise-induced transitions discussed by Horsthemke and Lefever.[3] The locus of the roots of Eq. (1.10) for $\sigma\cong\sigma_c$ is shown in Fig. 1 by the solid curve along with some experimental measurements indicated by the triangles.

The statistical, stationary moments can be evaluated using Eq. (1.8), and the standard definition Eq. (1.6) then results in the equation of motion for the nth moment:

$$d\langle X^n\rangle_t/dt=nR\langle X^{n-1}\rangle_t-nQ\langle X^n\rangle_t+n\lambda\langle X^{n+1}\rangle_t-n[1-(\sigma^2/2)(n+1)]\langle X^{n+2}\rangle_t\,. \tag{1.11}$$

In the steady state this equation yields a recurrence relation for the moments, and hence we need only find the first two in order to obtain all of them. From Eq. (1.11) we see that the stationary n moments exist if $n\le n_0$ as shown by Eq. (1.9). From Eq. (1.6) we can also obtain the equation of motion satisfied by the correlation function

$$d\langle X(t)X(0)\rangle/dt=R\langle X\rangle_{\rm st}-Q\langle X(t)X(0)\rangle_{\rm st}+\lambda\langle X^2(t)X(0)\rangle_{\rm st}-(1-\sigma^2)\langle X^3(t)X(0)\rangle_{\rm st}\,. \tag{1.12}$$

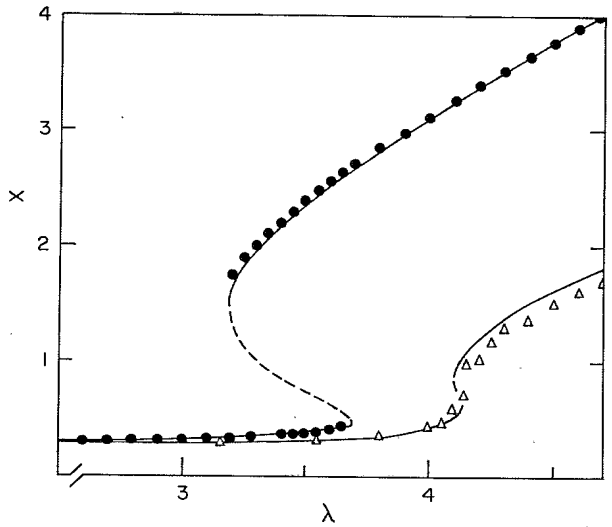

FIG. 1. Deterministic, steady-state values of X as obtained from Eq. (1.2) (solid curve) with measured values obtained from the circuit (closed circles) are shown on the left. On the right are the maxima X_m of $P_{\rm st}(X)$ as determined by Eq. (1.10) for $\sigma\simeq\sigma_c\simeq 1.0$ (solid curve) with measured values (open triangles).

This equation will be used in the Stratonovich approach in order to obtain T, as shown in Sec. III.

II. THEORETICAL BACKGROUND

In this section we present three very different methods for evaluating the relaxation time T. We have selected these because each of them yields a particular insight into the problem. The first one is valid for a monostable state, and it gives the upper bounds for T^{-1}. The second one was introduced by Stratonovich[23] and makes use of a decoupling in the equations for the correlations. This method can be understood as the lowest order of a more sophisticated approach.[17,24,25] We review this method here because it results in qualitatively correct predictions with minor effort. The last method, due to Jung and Risken, produces an exact result; however, the final formula, an integral, in almost all cases must be evaluated numerically.[19]

A. The deterministic approach

Let us suppose that σ is small so that the system is close to the deterministic state with only small fluctuations around this state. We define a change of variable

$$\Delta X=X-X_i\,, \tag{2.1}$$

where X_i is the deterministic value and ΔX is the fluctuation. Substituting Eq. (2.1) in (1.1) and retaining only linear terms, we get

$$\Delta\dot X=-(Q-2\lambda X_i+3X_i^2)\Delta X+X_i^2\xi(t)\,. \tag{2.2}$$

Because this equation is linear, the relaxation time is just

$$T^{-1}=Q-2\lambda X_i+3X_i^2\,. \tag{2.3}$$

This formula cannot be used in the bistable region, be-

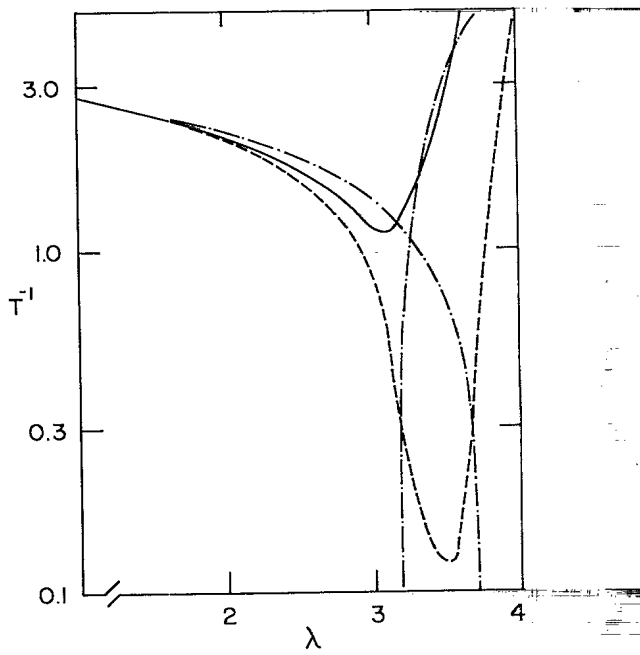

FIG. 2. Inverse relaxation time vs λ for different theories. The dot-dashed curve is the deterministic approximation obtained from Eq. (2.3). The solid curve is the prediction of the Stratonovich decoupling given by Eq. (2.8) with $\sigma=0.5$. The dashed curve is the Jung-Risken result for $\sigma=0.5$.

cause the steady state X_i is not unique (but see also below). In the monostable region it can be understood as the lowest order in a perturbation expansion in σ. So in principle we could expect good quantitative results, but only when both λ and σ are very small. This can be seen in Fig. 2, where the best agreement (with the results of the other two approaches) is obtained for small λ. If Eq. (2.3) is also applied in the bistable region, it yields two branches which cross each other within the region and finish at the boundaries determined by the limits of bistability as shown by the dot-dashed curves in Fig. 2.

B. The Stratonovich decoupling

The starting point for this method is Eqs. (1.11) and (1.12) which essentially involve an infinite hierarchy of equations for all the moments and correlations. Defining higher-order correlation functions by

$$C_n(t)=\langle X^{n-1}(t)X(0)\rangle_{st}-\langle X^{n-1}\rangle_{st}\langle X\rangle_{st} , \quad (2.4)$$

and using Eqs. (1.11) and (1.12), we obtain for $C_2(t)$

$$dC_2(t)/dt=-QC_2(t)+\lambda C_3(t)-(1-\sigma^2)C_4(t) . \quad (2.5)$$

The Stratonovich decoupling consists of expressing higher-order correlations in terms of the usual correlation function:

$$C_n(t)/C_n(0)=C_2(t)/C_2(0) , \quad \forall n , \quad (2.6)$$

which is exact in two limits, $t=0$ and $t=\infty$. This means that all the correlations relax on the same time scale. The result is a dynamical approximation in the sense that the decoupling affects Eq. (1.12) but not Eq. (1.11). The steady-state moments are not approximated, only the correlations.

Using Eq. (2.6) in (2.5), we obtain

$$dC_2(t)/dt=-[Q-\lambda C_3(0)/C_2(0)+(1-\sigma^2)C_4(0)/C_2(0)]C_2(t) \quad (2.7)$$

which is a linear equation of motion for $C_2(t)$ and hence implies that $C_2(t)$ relaxes exponentially with a relaxation time

$$T^{-1}=Q-\lambda C_3(0)/C_2(0)+(1-\sigma^2)C_4(0)/C_2(0) . \quad (2.8)$$

This expression depends on the first four steady-state moments. The first and second of these have been evaluated from Eq. (1.8) by the usual formula, using Romberg's numerical integration algorithm. The remaining two moments were obtained using Eq. (1.11); in particular,

$$\langle X^3\rangle_{st}=(1-\sigma^2)^{-1}(R-Q\langle X\rangle_{st}+\lambda\langle X^2\rangle_{st}) , \quad (2.9)$$

and

$$\langle X^4\rangle_{st}=(1-3\sigma^2/2)^{-1}(n\langle X\rangle_{st}-Q\langle X^2\rangle_{st}+\lambda\langle X^3\rangle_{st}) . \quad (2.10)$$

Because in this approximation for our model we require that the fourth moments be finite, the condition (1.9) results in an upper limit for σ:

$$\sigma<\sqrt{2/3}\simeq 0.815 . \quad (2.11)$$

In consequence, this method cannot be used for large values of σ.

Higher-order corrections can be defined and evaluated following standard approaches related to continued fraction methods,[17,24,25] but in some cases these corrections do not result in any substantial improvement.[9] Even worse, they can lead to nonphysical results as explained in Ref. 17. Nevertheless, the continued matrix fraction approach of Jung and Risken works very well for models with multiplicative noise.[19] In our opinion, the applicability of such nonstandard perturbative approaches depends strongly on the particular characteristics of the model: multiplicative or additive noise, divergences of the moments, etc.

In the present model there is no way to try to evaluate higher orders, because that would require the existence of higher-order moments[17,25] which in turn would further restrict the range of allowable values of σ. Thus better accuracy can be achieved only at the expense of the range of applicability. The relaxation time obtained from Eq. (2.8) with $\sigma=0.5$ is shown by the solid curve in Fig. 2.

C. The Jung-Risken method

Here we present a very brief review of the exact solution for the relaxation time as has recently been obtained.[19] The standard definition of the correlation function is

$$C_2(t)=\langle\Delta X(t)\Delta X(0)\rangle_{st}=\int dX_1\int dX_2\,\Delta X_1\,\Delta X_2\,P_2(X_1,t;X_2,0) , \quad (2.12)$$

where $\Delta X = X - \langle X \rangle$ and $P_2(X_1,t;X_2,0)$ is the joint probability, which can be expressed in terms of the conditional probability $P(X_1,t \mid X_2,0)$,

$$P_2(X_1,t;X_2,0) = P(X_1,t \mid X_2,0) P_{\rm st}(X_2) = e^{L(X_1)t} \delta(X_1 - X_2) P_{\rm st}(X_2) . \quad (2.13)$$

Substituting Eq. (2.13) into (2.12), and integrating out X_2, we have

$$C_2(t) = \int dX_1 \, \Delta X_1 \, W(X_1,t) , \quad (2.14)$$

where

$$W(X_1,t) = e^{L(X_1)t} \Delta X_1 \, P_{\rm st}(X_1) . \quad (2.15)$$

Now we time integrate Eq. (2.14) and, according to the definition of T, Eq. (1.4), we obtain

$$TC_2(0) = \int dX_1 \, \Delta X_1 \, \rho(X_1) , \quad (2.16)$$

where

$$\rho(X_1) = \int_0^\infty W(X_1,t) dt . \quad (2.17)$$

From Eq. (2.15) we observe that $W(X_1,t)$ obeys a Fokker-Planck–like equation of motion

$$\partial W(X_1,t)/\partial t = L(X_1) W(X_1,t) , \quad (2.18)$$

which is time integrated and according to the definition Eq. (2.17) yields

$$-W(X_1,0) = L(X_1) \rho(X_1) , \quad (2.19)$$

where $W(X_1,\infty) = 0$ from Eqs. (2.15) and (2.18). Equation (2.19) can now be integrated over X_1 between 0 and X to give

$$I(X) = -[f(X) + g'(X) g(X)] \rho(X) + \partial [g^2(X) \rho(X)]/\partial X , \quad (2.20)$$

where $f(X)$ and $g(X)$ are defined by (1.2),

$$I(X) = -\int_0^X \Delta X_1 \, P_{\rm st}(X_1) dX_1 , \quad (2.21)$$

and the integration constant was taken equal to zero.[19] Equation (2.20) is a linear, nonhomogeneous, ordinary differential equation for $\rho(X)$, which after integration gives

$$\rho(X) = P_{\rm st}(X) \int_0^X \frac{I(X')}{g^2(X') P_{\rm st}(X')} dX' , \quad (2.22)$$

where we have used the boundary condition $g^2(0)\rho(0) = 0$. Substituting Eq. (2.22) into (2.16) and integrating by parts,

$$T = \frac{1}{C(0)} \int_0^\infty \frac{I^2(X)}{g^2(X) P_{\rm st}(X)} dX , \quad (2.23)$$

which is the exact expression for T.

The dependence of T on the parameters λ and σ for this model have been explored following a numerical integration algorithm to evaluate Eq. (2.23). We briefly review the algorithm here. First we select an upper bound $X_{\rm max}$ for the integral in Eq. (2.23) and divide the domain of integration into 100 points. $I(X)$ is evaluated recurrently for each point,

$$I(X_{n+1}) = I(X_n) - \int_{X_n}^{X_{n+1}} \Delta X_1 \, P_{\rm st}(X_1) dX_1 , \quad (2.24)$$

where this integral is done by the six-point Gauss's formula.[26] The first moment in Eq. (2.24) ($\Delta X_1 = X_1 - \langle X \rangle$) was obtained by Romberg's method with enough precision, and it was also used for the second moment in $C_2(0)$. The integration of Eq. (2.23) was finally completed by use of the extended Simpson's rule.[26] In order to avoid systematic numerical errors, for some values of the parameters, T was evaluated for different values of $X_{\rm max}$ and also for various partitions of the interval. No appreciable error was found.

In Fig. 2 we plot the results of this approach for $\sigma = 0.5$ as shown by the dashed curve. All three methods can now be compared. In the monostable region for small enough λ, all three approaches are in agreement; however, there is substantial disagreement in the other monostable region because of the large values of λ. In the bistable region only the Stratonovich and Jung-Risken approaches can be used, and we shall show in Sec. III that of these two only the latter is in agreement with the measured results, at least to within the estimated experimental uncertainties. The Stratonovich decoupling predicts the minimum in T^{-1}, but the results are not quantitative. This is not surprising, because this approach does not take into account the dominant mechanism in the bistable region: the passage time from one well to the other and vice versa. This tendency to underestimate T was also observed in other, even more stable, systems.[25]

The minimum in T^{-1} is the dominant feature predicted by theory and is a good dynamical characterization of a noise-induced transition, since it clearly shows critical slowing down induced by varying either λ or σ. For a smaller value of σ ($\sigma = 0.2$) not plotted in Fig. 2, the minimum of T^{-1} decreases an order of magnitude more. Indeed, $T \to \infty$ in this model as $\sigma \to 0$, while no such singularity appears in the moments.[27–29]

III. THE EXPERIMENT

In order to test these theoretical predictions, we have also carried out a detailed experimental study of the relaxation time, based on the electronic circuit illustrated in diagrammatic form in Fig. 3. Its mode of operation, similar to that of some circuits described previously,[15,16,20,21,27] is as follows. For any given X, the various terms on the right-hand side of (1.1) are constructed in a sequence of arithmetic operations using standard analogue electronic components; the bandwidth-limited Gaussian white noise, with correlation time τ_N, is supplied from an external generator. The resultant time-varying signal, representing $F(X,t)$ for the cubic bistable defined by (1.2), with $Q = 3$ and $R = 0.7$, is integrated and then equated to X by being returned to the input, as shown.

The actual circuit used in practice differed in certain important respects from the idealized version shown in Fig. 3. One of these was that the integrator time constant τ_I was much less than unity. Some other variations were also necessary in order to obtain reliable data for particular ranges of σ, and we will refer to these below. The principal reason for making $\tau_I \ll 1$ is to shift the range of

frequencies ν that are of interest into a region where the power spectrum of a standard commercial noise generator is reasonably flat (since the response of most generators tails off rapidly for $\nu < 10$ Hz). Additional motivations were to simplify circuit design and to avoid the inordinately long data-acquisition periods that would have been entailed by a need to accommodate frequencies in the sub-Hertz range. The choice of $\tau_I \neq 1$ has two other direct consequences that must carefully be borne in mind. First, when bandwidth-limited white noise of rms voltage V_N and correlation time $\tau_N \ll \tau_I$ is being applied to the circuit, the quantity σ that appears in the white-noise equations above is then specified[30] by

$$\sigma = (2\tau_N/\tau_I)^{1/2} V_N \ . \tag{3.1}$$

Provided $\tau_N \ll \tau_I$, the noise is perceived by the circuit as effectively white and (3.1) remains valid. Second, there is an effective scaling of real time so that, to make our measurements of the relaxation time consistent with the theoretical discussion above, it is necessary to divide them all by τ_I. For most of the measurements, the time constants were $\tau_N = 59\ \mu$s, $\tau_I = 6.5$ ms.

The deterministic ($\sigma = 0$) response of the circuit is shown by the closed circles of Fig. 1, where it is also compared with the ideal behavior predicted by a solution of (1.2). The agreement obtained is not perfect, but the small discrepancies (typically a few percent) that are evident can readily be accounted for in terms of known nonidealities of the analogue components. The statistical density of X for $\sigma > 0$ has also been measured for this circuit and has been found to be in satisfactory agreement with the predictions of both (1.8) and (1.10): A comparison of the experimental data with (1.10) is shown for $\sigma \simeq 1.0$ by the triangles and associated solid curve in Fig. 1.

The relaxation time T of the system was determined for different values of λ and σ by means of a Nicolet 1080 computer system, through the application of a standard Fourier transform technique[31] for computation of the autocorrelation function that, in outline, was as follows. First, a sample of $X(t)$ was digitized at 1024 discrete points separated by a sample interval that was varied so as to suit the value of T that was to be measured. Second, a constant was added to every point in the block so as to obtain a function with zero mean. Third, after the provision of an adjacent block of 1024 zeros (to eliminate potential ambiguities arising from circular correlation effects) a fast Fourier transform was performed on the combined block. Fourth, the result was squared to give the power spectrum, following which, fifth, the inverse transform was taken to yield the autocorrelation function. After removal of the bias[31] resulting from the noninfinite size of the block, and after interchanging the left- and right-hand halves of the result, this procedure yielded the autocorrelation function $C_2(s)$ as defined by (1.5), with the zero of the offset time s referred to the center of the block. The whole sequence was repeated typically 200 times, the results being added and averaged so as to enhance their statistical reliability. Finally, a small baseline correction, again necessitated by the noninfinite length of the digitized blocks of $X(t)$, was implemented to ensure that the flat portion of $C_2(s)$ obtained for large s was centered accurately on zero.

Two typical results of these procedures are shown in Fig. 4, in each case for $\lambda = 3.6$. In the recording of Fig. 4(a) the noise level was sufficiently low ($\sigma = 0.1$) that X remained close to the upper root for the duration of the measurement. The resultant autocorrelation function is exponential within experimental error, as indicated by the linearity of its logarithm plotted in Fig. 4(b). For a larger noise level, where switching is taking place between the two states of the bistable, a much wider autocorrelation

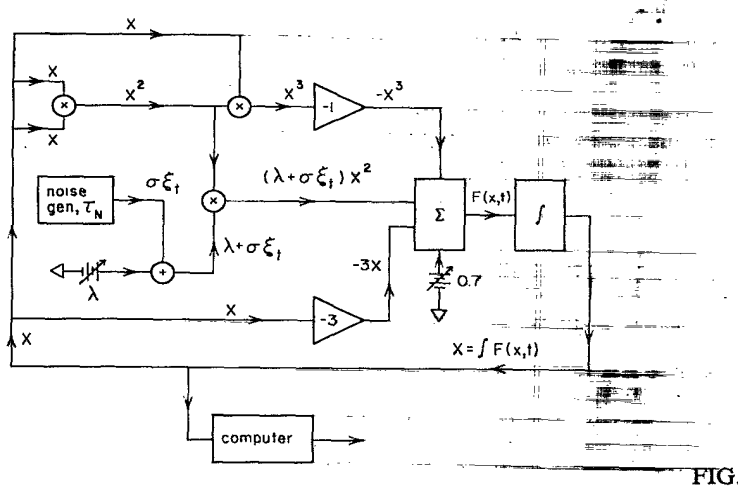

FIG. 3. Schematic diagram of the electronic circuit used for experimental measurements of the relaxation time T defined by (1.4). The computer acts purely as a measuring instrument and in no way affects the operation of the circuit.

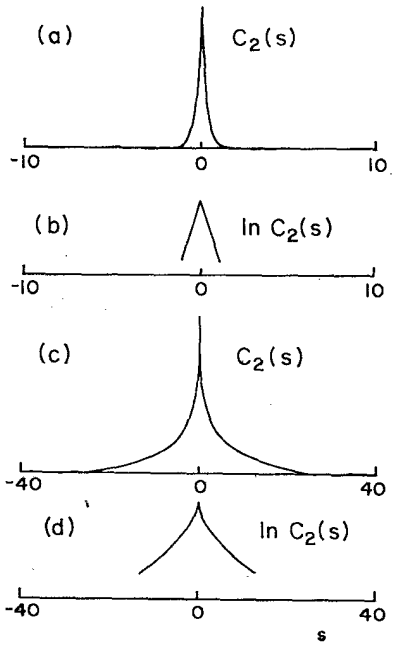

FIG. 4. Experimental autocorrelation functions $C_2(s)$ as defined by (1.5) measured at $\lambda = 3.6$. In (a), $C_2(s)$ is shown for $\sigma = 0.1$, and in (b) its logarithm is plotted. In (c), $C_2(s)$ is shown for $\sigma = 0.6$, and its logarithm, plotted in (d), shows that the behavior is then decidedly nonexponential in character.

function, as in Fig. 4(c), is obtained [where the change in the scale of s from Fig. 4(a) should be noted]. Under these conditions, the form of $C_2(s)$ is decidedly nonexponential, as shown by the nonlinear shape of its logarithm plotted in Fig. 4(d).

To evaluate the relaxation times, we have integrated the experimental correlation functions, in practice truncating the integrals at a value of s where $C_2(s)$ has fallen to zero and then dividing the result in each case by $C_2(0)$ thereby computing the relevant value of T in accordance with (1.4).

The principal obstacle to the acquisition of reliable data arises from the relatively very large breadths of the densities represented by (1.8) and the consequent difficulty of accommodating these within the limited dynamic range of standard electronic components. In recognition of this problem, we have introduced a number of modifications to the basic circuit shown in Fig. 3. The most important of these is a scaling down by a factor of 100 of the voltages in the section of the circuit prior to the summation amplifier and a subsequent multiplication of the integrated signal by 100 so as to ensure that the overall scale factor of the circuit remains equal to unity. A number of additional small modifications were required when $\sigma > 0.5$, to prevent or reduce clipping of the largest voltage excursions in the components that deal with X^2, and for σ up to the largest experimental value of $\sigma = 1.5$ it was also found necessary to alter the overall scale factor such that $X \rightarrow X/2$. After every modification the deterministic ($\sigma = 0$) response of the circuit was remeasured to ensure that the upper solid curve of Fig. 1 was still being followed.

The form of the circuit that was developed to cope with large values of σ turned out to be quite unsuitable for measurements with small σ (as well as vice versa). This was, in particular, because of the increased importance of small drifts in the values of λ and R and also because the intrinsic noise of the circuit components themselves could then become comparable with the external noise unless, of course, σ was relatively large. We have therefore used slightly different versions of the basic circuit to cover different ranges of σ: The data thereby obtained are consistent and agree with each other in the regions of overlap.

In view of the foregoing remarks, it is hardly necessary to emphasize that the circuit is a "real physical system" and therefore subject to the experimental errors and nonideal modes of behavior (as compared to the relevant model equations) that invariably characterize such systems. It should be noted, for example, that small drifts in λ and R due, perhaps, to changes in temperature are bound to result in large changes in T when the system is near an instability. To look at it in another way, quite small drifts of the circuit parameters can cause the exact location of the instability to alter, again resulting in relatively large changes in T.

Some of our experimental results are plotted, and compared in each case with the corresponding theoretical predictions, in Figs. 5–7. The random error in the data can best be judged by their departures from the curves drawn through them. The error bars on some of the points represent estimates of the uncertainty introduced by the small baseline correction referred to above; the nonideal responses of the analogue components contribute to additional systematic errors amounting typically to $\sim \pm 10\%$ and, in the worse cases, to $\sim \pm 30\%$ in T.

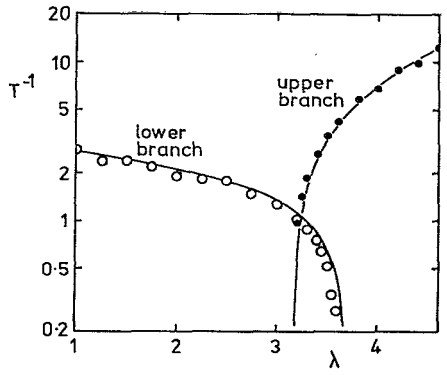

FIG. 5. Inverse relaxation times T^{-1} in the limit of very small σ, determined under conditions such that, within the bistable region, no switching occurred between the upper and lower states during the period necessary to complete the measurement. The curves represent (2.3).

The results in Fig. 5 refer to very small σ where (in practical terms, even within the bistable region) T^{-1} is effectively independent of σ, and the curves represent (2.3). The agreement between experiment and theory is excellent. That this should be so within the bistable region might at first seem surprising in light of the preceding theoretical discussion, because in principle $T \rightarrow \infty$ as $\sigma \rightarrow 0$, and, because, in any case, (2.3) is formally inappli-

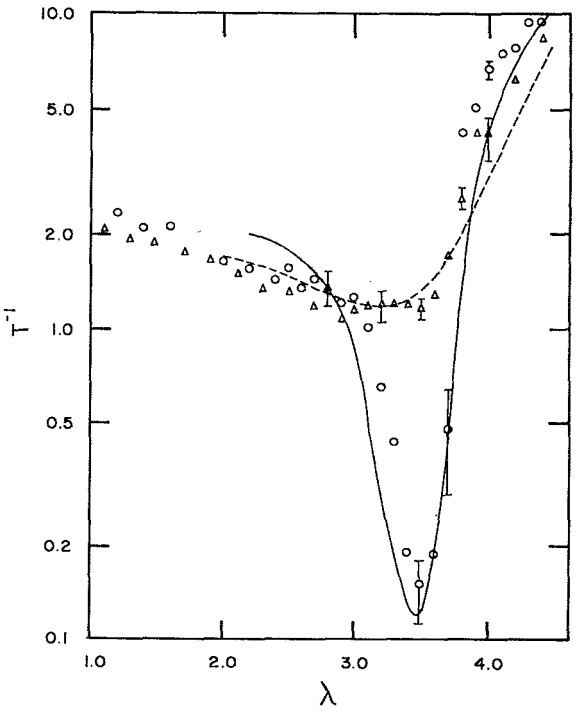

FIG. 6. Measured inverse relaxation times vs λ for $\sigma = 0.5$ (open circles) and $\sigma = 1.0$ (open triangles). The curves are the prediction of the Jung-Risken theory for the same values of σ.

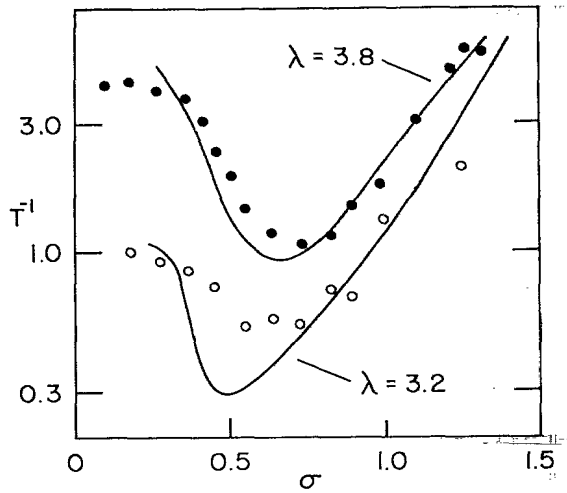

FIG. 7. Measured inverse relaxation times vs σ for values of λ as shown. The curves are the Jung-Risken results.

cable to cases where X_i is not unique. In practice, however, these experimental data were acquired under conditions such that no switching occurred during the period of time (typically 20 minutes) needed to complete a measurement of T, the system having previously been set in the chosen upper or lower state by an appropriate sequence of changes in λ. Thus, within the time scale of the measurements, X_i can be regarded as unique and (2.3) can properly be expected to apply, consistent with the results of Fig. 5.

For larger values of σ a pronounced minimum is found in $T^{-1}(\lambda)$ within the bistable regime, as shown in Fig. 6 for two values of σ. The experimental data (points) show a variation with λ that is very closely similar to the behavior predicted above (curves) on the basis of the Jung-Risken theory. Figure 7 shows a comparison between the measured (points) and predicted (curves) variation of T^{-1} with σ for two values of λ. Again, encouragingly close agreement is found between experiment and theory, there being pronounced minimum in $T^{-1}(\sigma)$ for both.

IV. CONCLUSIONS AND COMMENTS

We have shown, theoretically and experimentally, that it is possible to characterize a noise-induced transition by looking at the relaxation time of the fluctuations in the steady state. It had previously been established that no true phase transition would appear in a zero-dimensional system. That is true from a rigorous, equilibrium statistical mechanics point of view. But nonequilibrium systems need not be characterized only within the equilibrium framework. Here we have presented a real, physical, nonequilibrium system which exhibits a first-order transition driven by the external control parameters λ or σ. We have shown that for some values of λ, there is an unmistakable critical slowing down, whose magnitude depends on σ, in accord with theoretical predictions. From these data, it is possible to conclude that a noise-induced transition is present. Further, this characterization of the transition in terms of T is more nearly definitive than previous characterizations which were based on the appearance and locations of the extrema of $P_{st}(X)$,[3,27] but they have the same meaning.

We comment that the exact approach due to Jung and Risken offers the best method for the study of relaxation times, because explicit results can be obtained, even though numerically, with a high degree of accuracy and minor computational difficulties. These are clear advantages compared to the more usual perturbative methods, which restrict one to small σ, or to nonperturbative methods related to continued fractions.

Finally, we emphasize that this noise-induced transition, with characteristic critical slowing down, has been observed in a real, physical system, the electronic circuit, and therefore could not be the result of either a definition or an artifact of the theoretical model.

ACKNOWLEDGMENTS

We are grateful to Professor H. Risken for a stimulating discussion and for useful comments on this manuscript. One of us (J.M.S.) gratefully acknowledges support from the University of Missouri—St. Louis.

[1]J. M. Sancho, M. San Miguel, S. Katz, and J. D. Gunton, Phys. Rev. A 26, 1589 (1982).
[2]F. Moss and G. Welland, Phys. Rev. A 25, 3389 (1982).
[3]W. Horsthemke and R. Lefever, *Noise-Induced Transitions* (Springer, Berlin, 1984).
[4]P. Grigolini, J. Stat. Phys. 27, 283 (1982).
[5]P. Hänggi and H. Thomas, Phys. Rep. 88, 207 (1982).
[6]R. Landauer, Phys. Today 31 (No. 11), 23 (1978).
[7]R. Graham, Phys. Rev. A 25, 3234 (1982).
[8]R. Graham, M. Hohnerbach, and A. Schenzle, Phys. Rev. Lett. 48, 1396 (1982).
[9]S. Faetti, P. Grigolini, and F. Marchesoni, Z. Phys. B 47, 353 (1982).
[10]L. Lugiato, J. D. Farina, and L. M. Narducci, Phys. Rev. A 22, 253 (1980).
[11]S. N. Dixit and P. S. Sahni, Phys. Rev. Lett. 50, 1273 (1983).
[12]P. Lett, R. Short, and L. Mandel, Phys. Rev. Lett. 52, 341 (1984).
[13]R. F. Fox, G. E. James, and R. Roy, Phys. Rev. A 30, 2482 (1984).
[14]P. Hänggi and F. Moss, in *Proceedings of the International Conference on Instabilities and Dynamics of Lasers and Nonlinear Optical Systems, Rochester, 1985,* edited by N. B. Abraham and R. W. Boyd (Cambridge University Press, Cambridge, England, in press).
[15]J. Smythe, F. Moss, P. V. E. McClintock, and D. Clarkson, Phys. Lett. 97A, 95 (1983).
[16]P. Hänggi, T. J. Mroczkowski, F. Moss, and P. V. E. McClintock, Phys. Rev. A 32, 695 (1985).
[17]A. Hernandez-Machado, M. San Miguel, and J. M. Sancho, Phys. Rev. A 29, 3388 (1984); Z. Rácz, Phys. Rev. B 13, 263 (1976).

[18]R. L. Statonovich, *Topics in the Theory of Random Noise, Vol. I* (Gordon and Breach, New York, 1963).
[19]P. Jung and H. Risken, Z. Phys. B **59**, 469 (1985); A. Szabo, K. Schulten, and Z. Schulten, J. Chem. Phys. **72**, 4350 (1980).
[20]P. V. E. McClintock and F. Moss, Phys. Lett. **107A**, 367 (1985).
[21]S. D. Robinson, F. Moss, and P. V. E. McClintock, J. Phys. A **18**, L89 (1985).
[22]G. V. Welland and F. Moss, Phys. Lett. **89A**, 273 (1982).
[23]R. L. Stratonovich, *Topics in the Theory of Random Noise, Vol. II* (Gordon and Breach, New York, 1967).
[24]S. Grossman, Phys. Rev. A **17**, 1123 (1978).
[25]P. Hänggi, A. Bulsara, and R. Janda, Phys. Rev. A **22**, 671 (1980).
[26]*Handbook of Mathematical Functions,* edited by M. Abramowitz and I. A. Stegun (Dover, New York, 1965), Chap. 25
[27]J. Smythe, F. Moss, and P. V. E. McClintock, Phys. Rev. Lett. **51**, 1064 (1983).
[28]H. R. Brand, Phys. Rev. Lett. **54**, 605 (1985).
[29]F. Moss, P. V. E. McClintock, and W. Horsthemke, Phys. Rev. Lett. **54**, 606 (1985).
[30]D. K. Kondepudi, F. Moss, and P. V. E. McClintock, Physica D (to be published).
[31]K. G. Beauchamp and C. K. Yuen, *Digital Methods for Signal Analysis* (Allen and Unwin, London, 1979).